AGU PUBLICATIONS

JGR

Journal of Geophysical Research: Space Physics

RESEARCH ARTICLE
10.1002/2014JA020903

Key Points:
- Na^+ can contribute up to ~30% of Mercury's plasma sheet thermal pressure
- K-H wave frequencies can correlate with the local Na^+ gyrofrequency
- K-H at Mercury transitions from MHD to kinetic scale across the dusk terminator

Correspondence to:
D. J. Gershman,
djgersh@umich.edu

Citation:
Gershman, D. J., J. M. Raines, J. A. Slavin, T. H. Zurbuchen, T. Sundberg, S. A. Boardsen, B. J. Anderson, H. Korth, and S. C. Solomon (2015), MESSENGER observations of multiscale Kelvin-Helmholtz vortices at Mercury, *J. Geophys. Res. Space Physics*, *120*, 4354–4368, doi:10.1002/2014JA020903.

Received 1 DEC 2014
Accepted 13 APR 2015
Accepted article online 16 APR 2015
Published online 4 JUN 2015

MESSENGER observations of multiscale Kelvin-Helmholtz vortices at Mercury

Daniel J. Gershman[1,2], Jim M. Raines[2], James A. Slavin[2], Thomas H. Zurbuchen[2], Torbjörn Sundberg[3], Scott A. Boardsen[4,5], Brian J. Anderson[6], Haje Korth[6], and Sean C. Solomon[7,8]

[1]Geospace Physics Laboratory, NASA Goddard Space Flight Center, Greenbelt, Maryland, USA, [2]Department of Atmospheric, Oceanic and Space Sciences, University of Michigan, Ann Arbor, Michigan, USA, [3]School of Physics and Astronomy, Queen Mary University of London, London, UK, [4]Heliophysics Science Division, NASA Goddard Space Flight Center, Greenbelt, Maryland, USA, [5]Goddard Planetary Heliophysics Institute, University of Maryland, Baltimore County, Baltimore, Maryland, USA, [6]The Johns Hopkins University Applied Physics Laboratory, Laurel, Maryland, USA, [7]Lamont-Doherty Earth Observatory, Columbia University, Palisades, New York, USA, [8]Department of Terrestrial Magnetism, Carnegie Institution of Washington, Washington, District of Columbia, USA

Abstract Observations by the MErcury Surface, Space ENvironment, GEochemistry, and Ranging (MESSENGER) spacecraft in Mercury's magnetotail demonstrate for the first time that Na^+ ions exert a dynamic influence on Mercury's magnetospheric system. Na^+ ions are shown to contribute up to ~30% of the ion thermal pressure required to achieve pressure balance in the premidnight plasma sheet. High concentrations of planetary ions should lead to Na^+ dominance of the plasma mass density in these regions. On orbits with northward-oriented interplanetary magnetic field and high (i.e., $>1\,cm^{-3}$) Na^+ concentrations, MESSENGER has often recorded magnetic field fluctuations near the Na^+ gyrofrequency associated with the Kelvin-Helmholtz (K-H) instability. These nightside K-H vortices are characteristically different from those observed on Mercury's dayside that have a nearly constant wave frequency of ~0.025 Hz. Collectively, these observations suggest that large spatial gradients in the hot planetary ion population at Mercury may result in a transition from a fluid description to a kinetic description of vortex formation across the dusk terminator, providing the first set of truly multiscale observations of the K-H instability at any of the diverse magnetospheric environments explored in the solar system.

1. Introduction

The temporal and spatial scales of charged particles in plasmas dictate their relevant physical regime and dominant physical processes. At the kinetic scale, individual charged particles gyrate about a magnetic field **B** with a characteristic time scale—given by the reciprocal of the gyrofrequency, $f = B/[2\pi\ (m/q)]$—and a characteristic spatial scale—given by the gyroradius, $r_g = (m/q)v/B$, where m/q is a particle's mass-per-charge ratio and v is its velocity perpendicular to **B**. At the fluid scale, all ions move collectively together with temporal and spatial scales that are much greater than those of an individual particle's gyromotion. Mercury's miniature magnetosphere, for which spatial scales can be comparable with a planetary ion gyroradius [*Russell et al.*, 1988; *Glassmeier et al.*, 2007], presents an opportunity to study a macroscopic system that can exhibit both kinetic and fluid behaviors. Since its orbital insertion in March 2011, the MErcury Surface, Space ENvironment, GEochemistry, and Ranging (MESSENGER) spacecraft [*Solomon et al.*, 2001] has been conducting regular observations of Mercury's space environment, with magnetic field and ion plasma measurements from the Magnetometer (MAG) [*Anderson et al.*, 2007] and Fast Imaging Plasma Spectrometer (FIPS) sensors [*Andrews et al.*, 2007], respectively.

Solar wind H^+ dominates the global plasma environment of Mercury [*Zurbuchen et al.*, 2008, 2011; *Raines et al.*, 2011, 2013; *Gershman et al.*, 2014]. H^+ gyromotions are well contained within a sizeable fraction of Mercury's magnetosphere, resulting in global, fluid-like behavior such as the formation of diamagnetic depressions in the magnetic cusp and central plasma sheet regions [*Ness et al.*, 1974; *Ogilvie et al.*, 1974; *Winslow et al.*, 2012, 2014; *Korth et al.*, 2011, 2012, 2014]. Many large-scale structures of the magnetosphere have been successfully reproduced by global simulations using both magnetohydrodynamic (MHD) [*Kabin et al.*, 2008; *Benna et al.*, 2010] and hybrid techniques [*Wang et al.*, 2010; *Trávníček et al.*, 2010; *Schriver et al.*, 2011]. Some features, such as the preferential formation of Kelvin-Helmholtz (K-H) vortices along Mercury's duskside magnetopause (MP) [*Boardsen et al.*, 2010; *Sundberg et al.*, 2012], with a few also observed on the dawnside

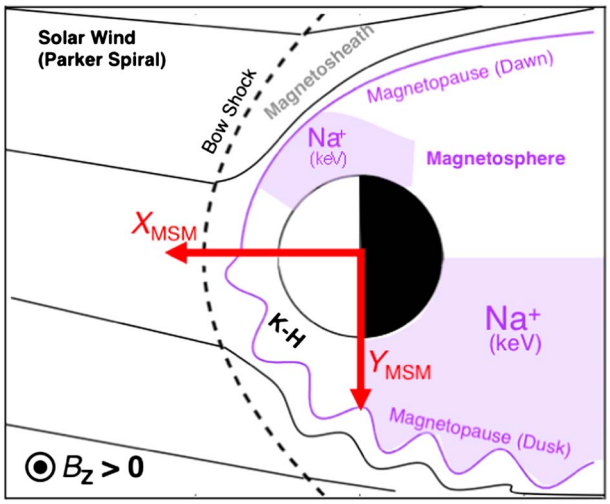

Figure 1. Illustration of Mercury's magnetosphere in the X_{MSM}-Y_{MSM} equatorial plane. The solar wind magnetic field (solid black lines) drapes around Mercury's magnetopause (solid purple line) downstream of a fast-mode bow shock (dashed black line). K-H vortices have been observed nearly exclusively on Mercury's duskside magnetopause on both the dayside and nightside when the IMF is strongly northward, i.e., $B_Z > 0$. Relatively high fluxes of keV Na^+ are observed near the dawn terminator and from dusk to midnight.

MP [*Liljeblad et al.*, 2014] (Figure 1), have been linked to kinetic scale plasma physics [*Nakamura et al.*, 2010; *Paral and Rankin*, 2013]. These large-scale (comparable to a Mercury radius, R_M, or 2440 km) K-H vortices may be capable of transporting substantial quantities of mass and energy between the solar wind and Mercury's magnetosphere, as has been observed at other planetary systems [e.g., *Lee et al.*, 1981; *Hasegawa et al.*, 2004; *Masters et al.*, 2010; *Wilson et al.*, 2012; *Delamere et al.*, 2013].

Planetary ions such as Na^+, with higher m/q than H^+, often have gyroradii that are on the same scale as spatial changes in Mercury's magnetospheric fields, enabling energization via nonadiabatic motion, in particular centrifugal acceleration [*Delcourt et al.*, 2003]. Low-energy (~100 eV) Na^+ ions outflowing from the cusp [*Raines et al.*, 2014] reach keV energies with trajectories that converge in the premidnight plasma sheet [*Raines et al.*, 2013; *Gershman et al.*, 2014] (Figure 1). Lower-energy (~0.1–1 eV) Na^+ ions photoionized from Mercury's neutral exosphere are expected to be abundant throughout Mercury's magnetosphere, especially on the dayside, but are not detectable by FIPS because of their low energies. These low-energy ions will have much smaller gyroradii than the hot (keV) H^+ ions in Mercury's magnetotail. However, some keV Na^+ ions have been observed in Mercury's equatorial dayside magnetosphere, mostly between 03:00 and 09:00 local time (LT) (Figure 1) [*Raines et al.*, 2013, 2014].

Numerical simulations of planetary ion trajectories [*Delcourt et al.*, 2003; *Seki et al.*, 2013; *Delcourt*, 2013] have treated Na^+ ions as independent test particles, although planetary ions have been reported in sufficient abundance (e.g., 0.1–1 cm^{-3} in the premidnight plasma sheet) [*Gershman et al.*, 2014] to contribute to bulk plasma parameters such as thermal pressure ($\Sigma_i P_i$), mass density ($\Sigma_i m_i n_i$), and instability growth, where n_i, P_i, and m_i are the number density, partial pressure, and mass of each species i in a plasma. Furthermore, it is in regions containing keV Na^+ ions that we expect kinetic scale physics to be most prominent. However, the collective behavior (i.e., contribution to bulk plasma properties) of planetary ions at Mercury, either at the kinetic or fluid scale, has not yet been verified with spacecraft observations.

Here we report the first direct and observable evidence for the dynamic influence of planetary ions in Mercury's magnetosphere. In section 2, we describe the selection and analysis techniques we applied to the MESSENGER data set. In section 3, we demonstrate that Na^+ contributes to the ion thermal pressure in Mercury's plasma sheet, confirming the influence of Na^+ in this region. Finally, in section 4, we show a distinctive behavior of the K-H instability at Mercury across the dusk terminator, where the observed period of K-H waves correlates with that of the local Na^+ gyroperiod. Additional discussion of the observations is given in section 5.

2. Data Selection and Analysis

For this study we used FIPS burst-mode data collected at ~10 s intervals from energy-per-charge (E/q) measurements between 100 eV/e and 13.3 keV/e and magnetic field vectors collected at 20 samples per second by MAG. Data were examined from 598 orbits between April 2011 and February 2013 during periods when MESSENGER passed through the dayside (14:00–16:00 LT) and nightside (18:00–21:00 LT) plasma sheets on its outbound (i.e., magnetosphere to magnetosheath or MS to MSH) or inbound

(i.e., MSH to MS) legs, respectively. These orbits also passed through Mercury's dusk magnetopause. Analogous data from orbits passing through Mercury's dawn magnetopause, also examined, were not used in this analysis because of the absence of abundant Na^+ or frequent evidence for K-H vortices [*Raines et al.*, 2013; *Liljeblad et al.*, 2014]. Instead, we focus on the differences between the dayside and nightside of the dusk terminator, where there is a strong spatial gradient in Na^+ content. We make use here of the Mercury solar magnetospheric (MSM) coordinate system, in which the origin is the locus of the internal field dipole, the X axis is directed parallel to the Mercury-Sun line, the Z axis is directed northward along the planet's rotation axis, and the Y axis completes the right-handed coordinate system; i.e., the X–Y plane is offset northward from the center of the planet by ~0.2 R_M along Mercury's spin axis [*Anderson et al.*, 2011].

FIPS is a time-of-flight mass spectrometer capable of resolving both solar wind (e.g., H^+ and He^{2+}) and planetary ion species (e.g., Na^+-group ions, defined as m/q between 21 and 30 amu/e) [*Zurbuchen et al.*, 2011]. The incident directions of ions within an instantaneous field of view (FOV) of ~1.15π sr are mapped onto a position-sensing anode with an angular resolution of ~15°, enabling analysis of the three-dimensional distribution functions for all species. For the subsonic velocity distribution function found in Mercury's plasma sheet, FIPS E/q distributions can be used to infer the density and temperature of both H^+- and Na^+-group ions [*Gershman et al.*, 2014]. Estimates of the plasma bulk speeds and temperatures, but not densities, can be recovered from supersonic flows such as the upstream solar wind or MSH flanks [*Gershman et al.*, 2012, 2013].

For identification of wave modes at the Na^+ gyrofrequency, we require 4–5 wave periods, setting a minimum of ~5 min to the interval needed to resolve the frequency range of interest [*Boardsen and Slavin*, 2007]. Therefore, given the short duration of MESSENGER transits through the plasma sheet, an interval of 5 min was used for spectral analysis. To determine the mean field direction for each time-centered 5 min window, a second-order polynomial was fit to each individual magnetic field component and used to detrend the data. A local coordinate system was used with unit axes $\mathbf{n}_1$, $\mathbf{n}_2$, and $\mathbf{n}_3$ defined such that $\mathbf{n}_3$ is parallel to the mean field, $\mathbf{n}_1 = \mathbf{n_3} \times \boldsymbol{Y}_{\mathbf{MSO}}$, where $\boldsymbol{Y}_{\mathbf{MSO}}$ is the unit vector in the Y_{MSO} direction, and $\mathbf{n}_2$ completes the right-handed system. The measured magnetic field vector (B_X, B_Y, and B_Z) at 20 samples per second was transformed into this coordinate system to form a time series of B_1, B_2, and B_3. A fast Fourier transform (FFT) of each component was computed to calculate perpendicular and parallel power spectral density (PSD) as ½($PSD_1 + PSD_2$) and PSD_3, respectively. The polarization was also calculated from B_1 and B_2. The derived spectral properties were smoothed over three adjacent frequency bins to aid in the identification of peaks. For quantitative analysis, only a single 5 min window was considered at a time, so spectral artifacts resulting from different detrending polynomials in adjacent time windows are negligible.

3. Na^+ Contribution to Bulk Plasma Properties

FIPS and MAG data measured during three transits by MESSENGER through Mercury's premidnight plasma sheet are shown in Figure 2. The MP crossing by the MESSENGER spacecraft from the MSH into the MS is indicated with a vertical dashed line and is accompanied by a change in the temperature of H^+ ions (first row), increased pressures of hot (~keV) Na^+-group ions (second and third rows), and diamagnetic depressions in the magnetic field (fourth row). The calculated thermal pressures for H^+- (P_{H+}) and Na^+-group (P_{Na+}) ions, as well as their contribution to the total tail pressure, are shown in Figure 2 (third and fourth rows), respectively. The magnetic pressure (P_B) is reduced to ~0.1 nPa because of the presence of thermal plasma (fourth row). The pressures P_B, P_{H+}, and P_{Na+} are calculated at time resolutions of 0.05 s, 30 s, and 90 s, respectively. P_{H+} is scaled by a factor of 1.1 to account for the pressure of heavier solar wind ion species [*Gershman et al.*, 2014]. Total pressures are calculated from data averaged to the contribution with the lowest time resolution. In addition to variations in the total pressure from magnetospheric dynamics [*Slavin et al.*, 2010a], increased Na^+ pressures are correlated with decreases in the H^+ pressures, an effect that is most pronounced in Figure 2b. As the local Na^+ pressure increases, the plasma sheet must expand and rarefy to maintain pressure balance with the tail lobes. This effect is consistent with previous surveys of Mercury's magnetotail, where increasing average Na^+ content from dawn to dusk [*Raines et al.*, 2013] is accompanied by decreased overall H^+ pressures measured over a wider band of magnetic latitudes [*Korth et al.*, 2014].

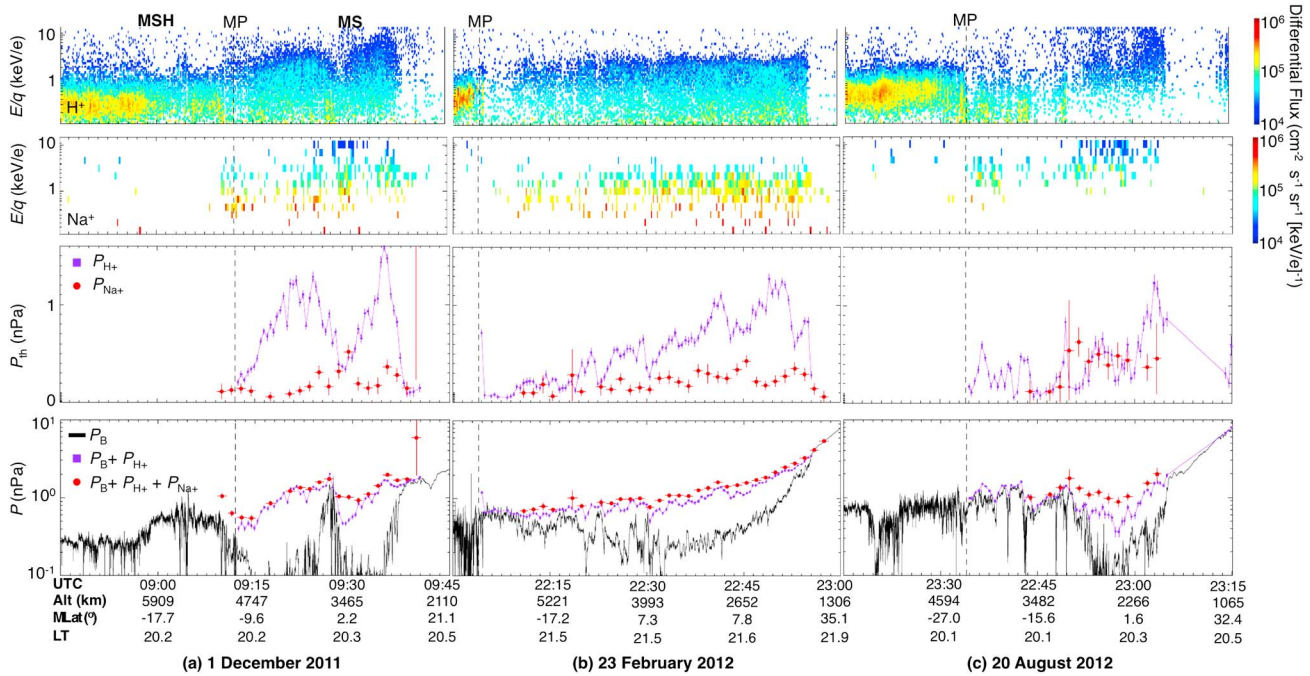

Figure 2. (top to bottom) H^+ *E/q* spectrogram, Na^+-group *E/q* spectrogram, plasma thermal pressures, and total magnetic field and plasma pressures for plasma sheet transits on (a) 1 December 2011, (b) 23 February 2012, and (c) 20 August 2012. Na^+ ion fluxes are averaged over four energy steps and two time steps to aid spectrogram visibility. The vertical error bars represent the effect of counting uncertainties on recovered plasma parameters [*Gershman et al.*, 2013]. Enhanced Na^+ pressures coincide with decreases in the H^+ thermal pressure and combine with P_B to provide total tail pressures of ~1 nPa.

The assumption of hot Maxwell-Boltzmann-like distributions for Na^+ was previously justified from data summed over many MESSENGER orbits [*Gershman et al.*, 2014] in order to accumulate a sufficient number of counts. For events with large, continuously measured Na^+ fluxes, however, such as those in Figure 2, we can examine the three-dimensional structure at much shorter time scales. As an example, in Figure 3, *E/q* distributions and all-sky maps [*Gershman et al.*, 2014; *Raines et al.*, 2014] of Na^+ flux are shown in the instrument frame for each event. The limited FOV of FIPS convolved with an average duskward drift of planetary ions [*Gershman et al.*, 2014] limits the quantitative evaluation of temperature anisotropy for Na^+ in this region. However, the Na^+ angular distribution functions appear hot and relatively isotropic in the instrument frame, consistent with the longer time accumulations and the assumptions made here to derive density and temperature. For these events, the average Na^+ density and temperature are n~1 cm^{-3} and T~15 MK, respectively.

4. Na^+ Influence on the K-H Instability

If the thermal pressure of the Na^+ ions is sufficient to generate diamagnetic depressions in Mercury's plasma sheet, then it may also influence the local plasma mass density and, consequently, the growth and evolution of instabilities. The ion cyclotron wave mode, for instance, has been identified at Mercury for H^+ [*Fairfield and Behannon*, 1976; *Boardsen et al.*, 2012]. Although the wave power of turbulence attributed to all ion scales (e.g., kinetic, multifluid, and MHD) is maximized in Mercury's plasma sheet [*Uritsky et al.*, 2011; *Boardsen et al.*, 2012], no distinct Na^+ ion cyclotron wave modes have been identified in the MESSENGER data set. Ion cyclotron wave modes are often generated from distribution function anisotropies [*Gary et al.*, 1993]. Their absence is therefore consistent with the relatively isotropic Na^+ ion distribution observed in this region, although FIPS may not be able to resolve small-temperature anisotropies, e.g., $T_\perp/T_\parallel < 2$, where $T_\perp$ and $T_\parallel$ denote the temperature perpendicular and parallel to the magnetic field direction, respectively. In addition, the transient nature of the observed Na^+ ion fluxes (e.g., Figure 2) may also limit our ability to obtain the 4–5 wave periods necessary to identify the Na^+ ion cyclotron wave mode in this region [*Boardsen and Slavin*, 2007].

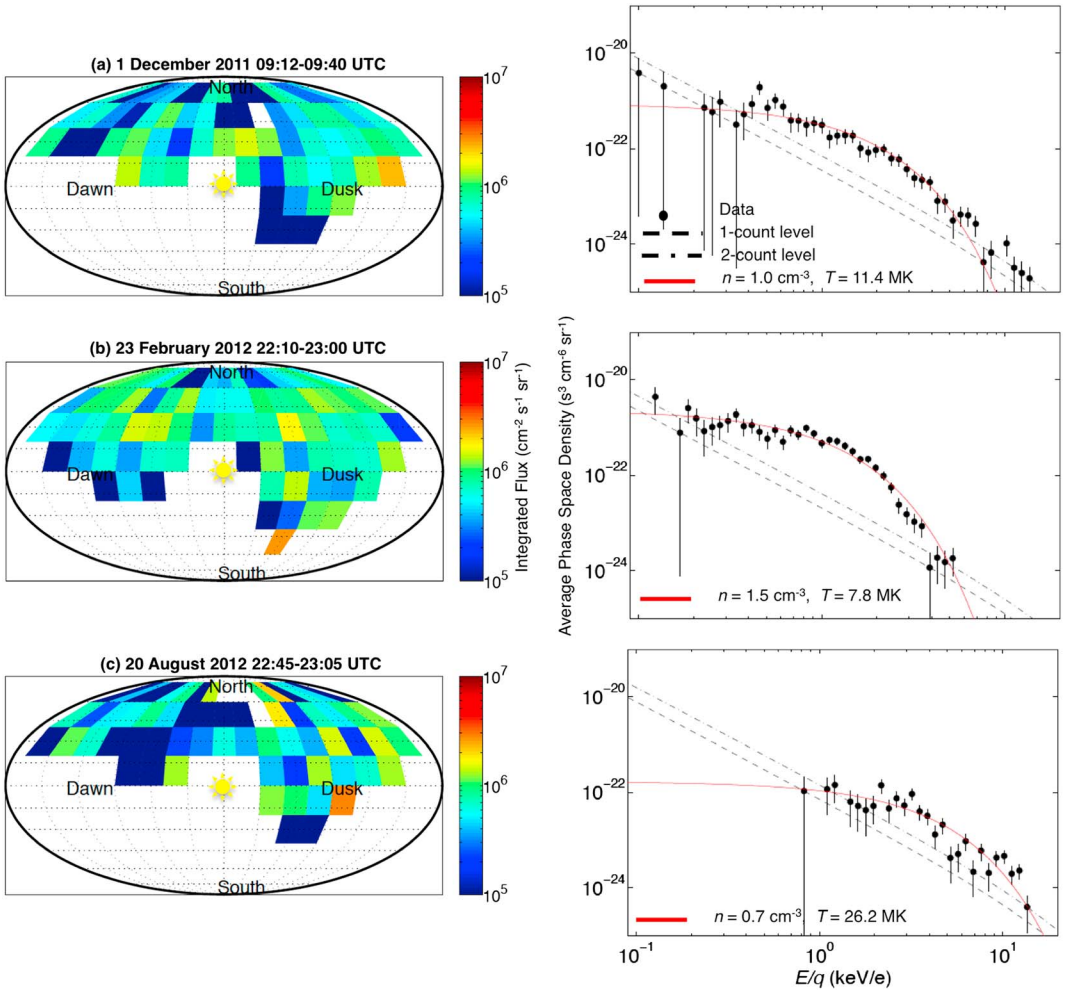

Figure 3. (left) All-sky map of integrated flux (in units of cm^{-2} s^{-1} sr^{-1}) of Na^+ with 15° angular binning. The Sun symbol at the center of each projection indicates particles flowing antisunward. Additional details on the construction of sky maps from FIPS measurement have been described by *Raines et al.* [2014] and *Gershman et al.* [2014]. (right) *E/q* phase-space distribution of Na^+ averaged over the FIPS FOV (~1.15π sr) for selected intervals from Figure 2, with (a), (b), and (c) corresponding to their counterparts in Figure 2. The black dashed and dash-dotted lines show the 1-count and 2-count sensitivity limits of FIPS for these intervals for an isotropic input distribution. The solid red line corresponds to the effective isotropic and stationary (in the instrument frame) Maxwell-Boltzmann distribution that was derived from moments of the accumulated *E/q* distributions. The Na^+ distributions are all consistent with hot (~keV) and dense (~1 cm^{-3}) distributions.

Unlike a clear signature of the Na^+ ion cyclotron wave mode, the K-H instability has been observed on both the dayside and nightside of Mercury's dusk terminator [*Sundberg et al.*, 2012; *Liljeblad et al.*, 2014]. The strong spatial gradient in keV Na^+ content across the terminator could result in a characteristic difference between vortices observed on the dayside and nightside. Numerical simulations of K-H vortices [*Nakamura et al.*, 2010] have demonstrated that a transition from the kinetic scale to the MHD-scale K-H instability occurs when the thermal ion gyroradius is of the same spatial scale (L) as the thickness of the MP boundary layer (BL) across the MSH-MS interface. Kinetic scale effects do not require nonthermal velocity distribution functions. Instead, the thermal gyroradius provides a threshold for which a sizeable fraction of an ion population gyrates on the spatial scale of the BL.

Along the duskside MP, the convective electric field points inward toward the MP, shrinking the thermal gyroradius (r_g) of ions crossing the BL by as much as a factor of 2. If this modified gyroradius (r_g') exceeds the initial half thickness (i.e., $L/2$) of the boundary, then the BL broadens to a thickness $L = 2\,r_g' \sim r_g$. Here r_g is the ion gyroradius measured inside the MS and is a factor of ~2 larger than the "effective gyroradius" as

defined by *Nakamura et al*. [2010]. The fastest-growing wavelength (λ_{KH}) for the Kelvin-Helmholtz instability is related to the boundary layer thickness by the relation λ_{KH}~$2\pi L$. For a thermal ion gyroradius much smaller than the observed BL thickness, i.e., $r_g << L$, an MHD description should be appropriate and $\lambda_{KH} >> r_g$. For r_g~L, in contrast, a kinetic description should be appropriate and λ_{KH}~$2\pi r_g$. Because the BL quickly (i.e., within only a few gyroperiods) grows to accommodate the gyro-orbit of the dominant ion, if we observe $r_g >> L$, then that ion species is likely not participating in K-H vortex formation. Similarly, for an infinitely thin BL but with the addition of a gyroviscous term to the ion pressure tensor, *Sundberg et al*. [2010] derived the dispersion relation for the K-H instability and found the wavelength of the fastest-growing wave mode to be λ_{KH}~$2\pi r_g$.

We may estimate the thermal Na^+ gyroradius inside the MS with MESSENGER data, but because we are limited to observations from only a single spacecraft, our estimation of L is subject to large uncertainties. The most robust available measurement of K-H phenomena is the frequency (f_{KH}) of magnetic fluctuations as vortices convect past the spacecraft. This frequency relates to the vortex wavelength by its center-of-mass speed (v_o) as λ_{KH}~v_o/f_{KH} [*Boardsen et al*., 2010; *Sundberg et al*., 2012]. Although direct measurements from FIPS of velocities in the BL are not available, from hydrodynamics we know that the MSH flow speed will scale with the upstream solar wind speed and increase from the dayside to the nightside [*Spreiter et al*., 1966].

For the case of equal mass densities in the MSH and MS, we expect that the vortex convection speed on the dayside will be a small fraction (~20%) of the upstream solar wind speed. On the nightside, the MSH flow speed will increase by as much as a factor of ~2. However, because of the contribution of Na^+ in the premidnight plasma sheet, the MS mass density will increase substantially, lowering the center-of-mass speed. It is therefore conceivable that the K-H vortex speed is broadly similar on either side of the dusk terminator. In addition, the thermal velocity of Na^+ in the premidnight plasma sheet (v_{th}) has been shown to scale as ~20% of the upstream solar wind speed [*Gershman et al*., 2014] so that v_{th}~v_o. The expected K-H wavelength can then be related to the Na^+ gyrofrequency, f_{Na+}, by

$$\lambda_{KH} \approx 2\pi r_g = \frac{2\pi v_{th}}{qB_{MP}} = \frac{v_{th}}{f_{Na+}} \approx \frac{v_o}{f_{Na+}}. \quad (1)$$

Therefore, the signature of gyro-orbit-size K-H vortices at Mercury should be magnetic fluctuations near the Na^+ gyrofrequency, i.e., a scaling of f_{KH} with B_{MP}. MHD-scale K-H fluctuations should not exhibit a similar B_{MP} dependence.

We must distinguish observations of K-H waves from other types of instabilities at Mercury that could produce fluctuations near the Na^+ gyrofrequency, in particular, the ion cyclotron instability. Resonant ion cyclotron wave modes such as those previously observed at Mercury for H^+ [*Fairfield and Behannon*, 1976; *Boardsen et al*., 2012] are left-hand polarized, a natural consequence of left-handed ion gyromotion. Some hot ion-ion beam instabilities can result in right-hand polarized fluctuations at the ion gyrofrequency but require near super-Alfvénic differential field-aligned flow between ion species [*Gary*, 1991]. K-H vortices result in velocity fluctuations, where on the duskside MP, i.e., a positive field-aligned vorticity case [*Nakamura et al*., 2010], the antisunward MSH flow "rolls up" into the MS in a right-handed sense compared with the mean flow direction. Because magnetic field lines are frozen into the vortex flow at low latitudes, these right-handed velocity fluctuations deform the local magnetic field [*Hasegawa et al*., 2004; *Faganello et al*., 2012]. Therefore, right-hand polarized fluctuations could be indicative of K-H vortices but not ion cyclotron waves. In addition, we expect a BL to form near the MP during K-H events that contain a mixture of MSH and MS plasma. These criteria will aid in the identification of K-H events in the MESSENGER data set on both the dayside and nightside. The field-aligned flow speeds of Na^+ and H^+ inside the MS are small, so Doppler shifts should not substantially influence our determination of wave period or polarization in the spacecraft frame. Furthermore, substantially Doppler-shifted ion cyclotron waves would not exhibit wave power clustered near the Na^+ gyrofrequency.

4.1. Dayside K-H Waves

K-H waves with frequencies f_{KH}~0.025 Hz are often observed on the dayside (~15:00 LT) of Mercury during intervals of northward-oriented interplanetary magnetic field (IMF), as shown by the three examples in

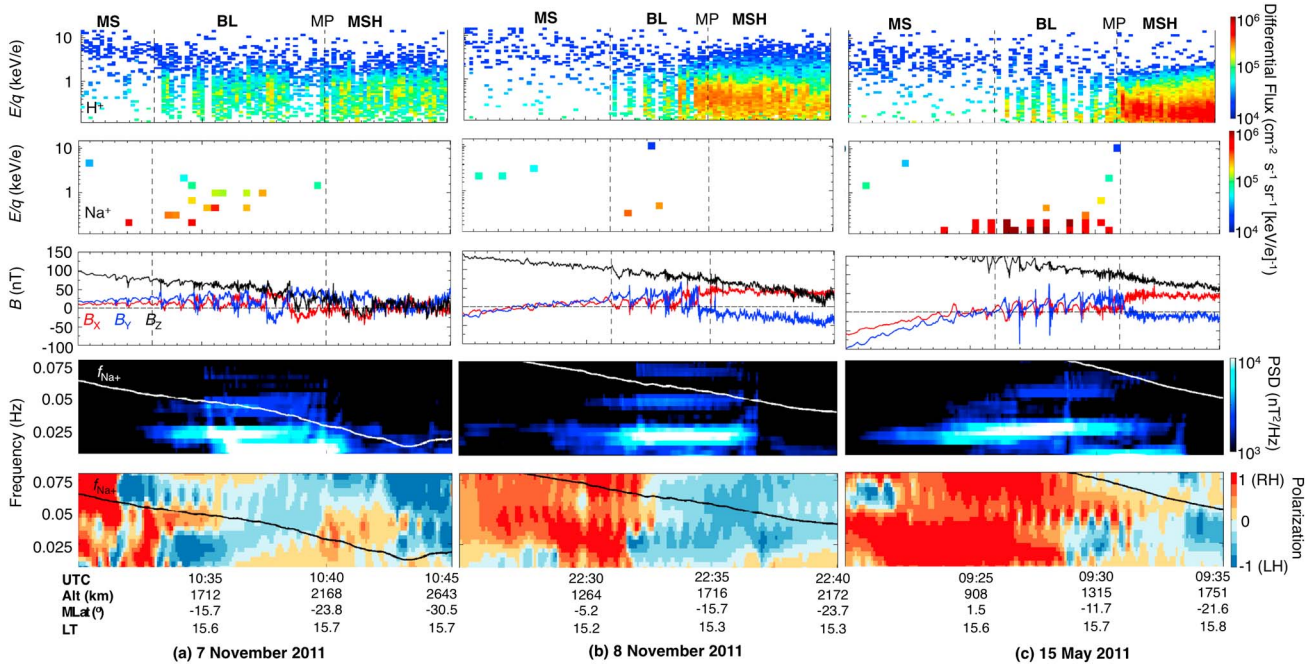

Figure 4. (top to bottom) H^+ *E/q* spectrogram, Na^+-group *E/q* spectrogram, magnetic field vector, power spectral density (PSD), and polarization of perpendicular fluctuations for dayside plasma sheet transits on (a) 7 November 2011, (b) 8 November 2011, and (c) 15 May 2011. Na^+ ion fluxes are averaged over four energy steps and two time steps to aid spectrogram visibility. A boundary layer with increased fluctuation power and mixed magnetosheath and magnetospheric plasma is observed for each orbit inside the MP; BL passage is delimited by vertical dashed lines. The dominant ion here is H^+; only modest amounts of keV Na^+ ions are seen. An average of B_{MP} over a sliding window 2.5 min in length is used to provide visualization of the Na^+ gyrofrequency as the solid white and black lines in the PSD and polarization panels, respectively. The peak fluctuation power in the magnetosphere does not vary with B_{MP} and is nearly steady in frequency at ~0.025 Hz (40 s period) for all cases.

Figure 4. For each example, there is a BL marked by multiple magnetopause crossings, a mix of MS and MSH material, and large-amplitude fluctuations in the magnetic field. In addition, the polarization of the fluctuations is right handed inside the MS. The K-H wave period as observed in the magnetic fluctuations is not a strong function of the magnetic field strength inside the BL, B_{MP}, which varied between ~60 and ~120 nT for these events.

Although there can be enhanced fluxes of Na^+-group ions measured near Mercury's dayside equator (Figure 4c), they are at substantially lower energies (~100 eV) than the hot (keV) plasmas observed farther downtail [*Gershman et al.*, 2014]. A wave frequency of ~0.025 Hz corresponds to a K-H wavelength of ~3000 km, on the order of a Mercury radius. The thermal gyroradius of the magnetospheric H^+ (T~20 MK) is ~50 km, which is an order of magnitude smaller than the thickness of the observed BL, estimated to be ~500 km on the basis of the change in spacecraft radial distance from the planet through this region. The Na^+ gyroradius in these regions for ion energies between 100 eV and 1 keV is 100–400 km, nearing the size of L. However, because the overall keV Na^+ content in this region is low, these relative scales suggest that a fluid-level (i.e., MHD) description of K-H may be appropriate on Mercury's dayside.

4.2. Nightside K-H Waves

K-H waves observed on the nightside (~20:00 LT) show distinct differences from their dayside counterparts, as demonstrated by the three events in Figure 5. For each event, in addition to the northward MSH field, mixed MS-MSH BL, and right-hand polarized fluctuations inside the MS, there are high concentrations ($>1\,cm^{-3}$) of keV Na^+-group ions in the plasma sheet. For the range of B_{MP} values on the nightside, the gyroradii of Na^+ are estimated to be ~500 km, on the same order as the thicknesses of the BL. L is estimated from the change in the Y_{MSM} coordinate across the BL. Here kinetic scale effects should become relevant. The observed wave frequency of K-H vortices, unlike the situation on the dayside, is

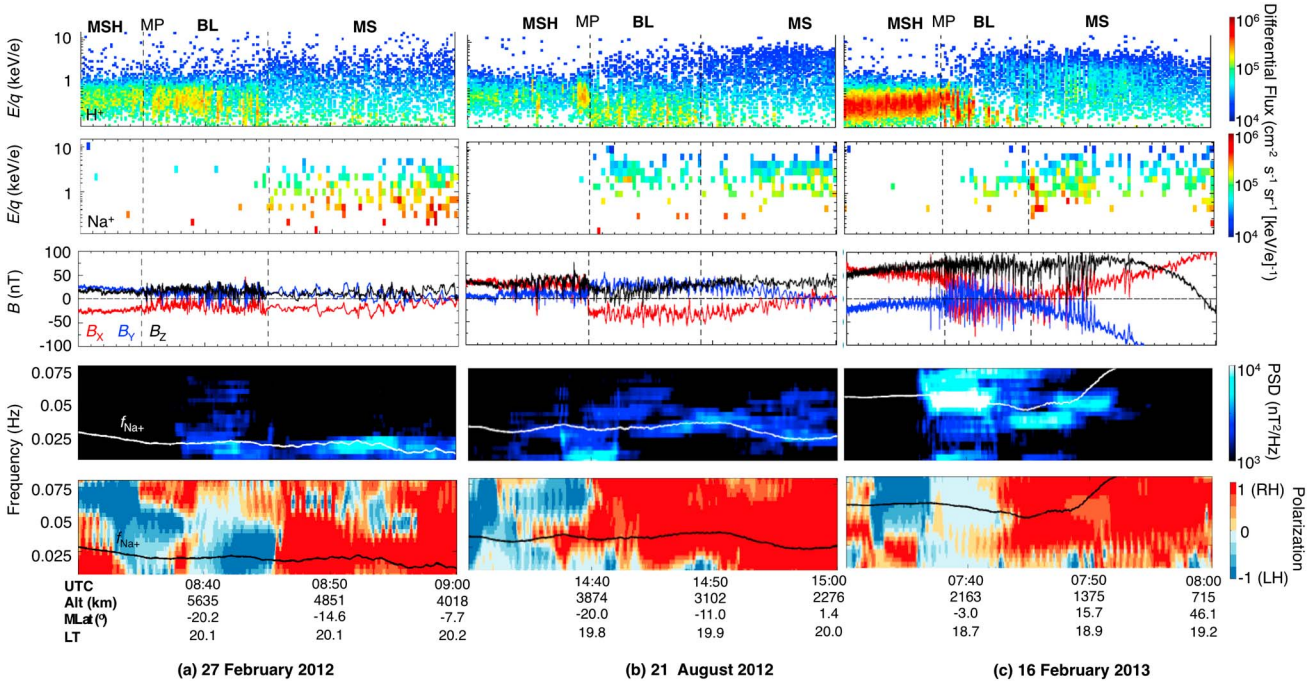

Figure 5. Same format as Figure 4 but for nightside plasma sheet transits on (a) 27 February 2012, (b) 21 August 2012, and (c) 16 February 2013. Here there are substantial fluxes of Na^+ ions measured in the magnetosphere. In addition, the fluctuations are in the magnetic field scale with B, matching the local Na^+ gyrofrequency (f_{Na+}). The fluctuations inside the magnetosphere are distinctly right-hand polarized.

approximately equal to the Na^+ gyrofrequency, with f_{KH}~0.01 Hz, 0.025 Hz, and 0.05 Hz for the events in Figures 5a, 5b, and 5c, respectively. These waves can extend well into both the MSH and the high-latitude MS [*Sundberg et al.*, 2012].

4.3. Survey of K-H Waves at Mercury

We have identified 25 and 33 MESSENGER orbits between April 2011 and February 2013 that contain signatures of K-H-like waves on Mercury's postnoon ($14:00 < LT < 16:00$) and premidnight ($18:00 < LT < 21:00$) magnetopause, respectively. These orbits represent 8% and 12% of those examined with MP crossings at these respective local times. K-H-like events were identified by large-amplitude fluctuations in the magnetic field near the MP that exhibit periodic nonsinusoidal (e.g., "sawtooth"-like) peak shapes, a northward MSH field ($B_Z > 0$), and a BL of MSH-MS plasma, i.e., no distinct boundary between the two populations. Orbits with substantial flux transfer event (FTE) activity, which can exhibit similar signatures, were excluded. In many cases, the precise bounds of the BL, in particular on the MSH edge, were difficult to determine because of unfavorable spacecraft orientation that prevented the bulk of the MSH flow from entering the FIPS aperture; best estimates were made for each. The mean and standard deviation of magnetic field magnitude inside the BL were used to provide estimates of B_{MP} and its uncertainty, respectively. FFTs of 5 min intervals of stable fluctuations near the MP were used to identify the fundamental frequency of oscillations, as shown in Figures 6 and 7 for the events in Figures 4 and 5, respectively. The uncertainty in the observed frequency is defined by the full width at half maximum (FWHM) of the spectral peak. Events with long (~60 s) wave periods were particularly difficult to characterize but nonetheless exhibit the aforementioned properties.

The time, location, range of observed frequencies, and B_{MP} values are listed in Tables A1 and A2 in Appendix A for the dayside and nightside events, respectively. When available, an estimate of the daily averaged upstream solar wind speed (v_{sw}), derived from data measured outside of Mercury's bow shock [*Gershman et al.*, 2012], is also included. The angle between **B** and the Z_{MSM} axis, θ_Z, is calculated from 5 min averages of MAG data in the MSH immediately adjacent to the BL. In addition, when available, the

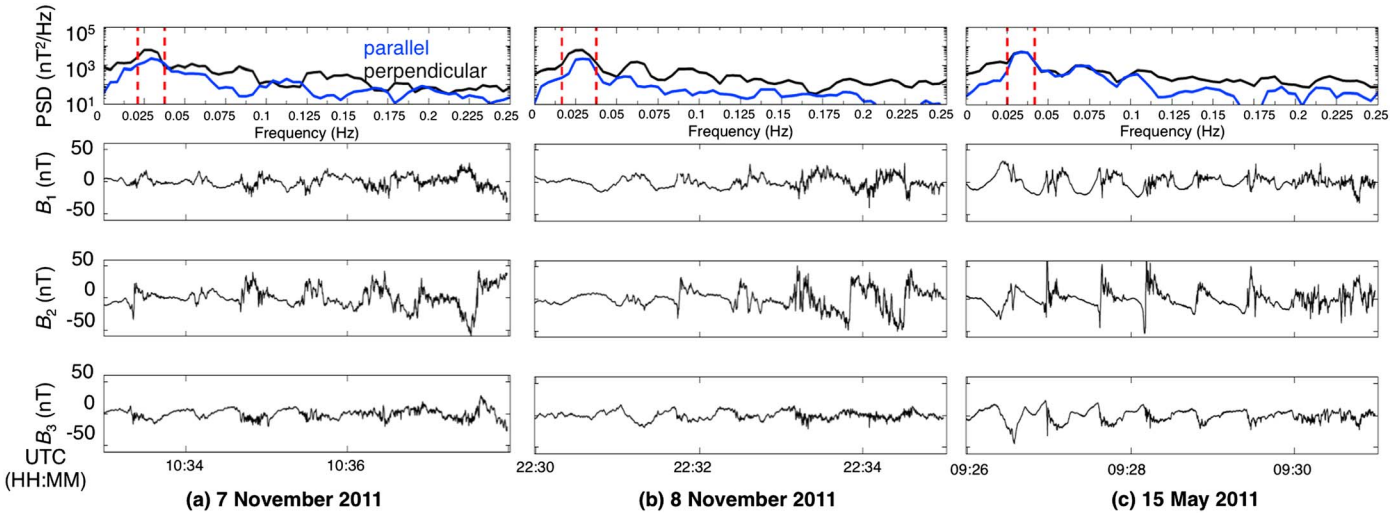

Figure 6. (first row) PSDs for parallel (blue) and perpendicular (black) fluctuations obtained from detrended values of B_1, B_2, and B_3 (second to fourth rows) for 5 min intervals during the dayside K-H events in Figure 4. The red dashed line indicates the FHWM of the lowest-order spectral peak.

densities and temperatures of H^+ and Na^+ in the plasma sheet were calculated for the nightside events from 5 min averages in the MS region immediately adjacent to the MP. Uncertainties in plasma densities and temperatures are based on counting statistics following *Gershman et al.* [2013]. Finally, the start time of the 5 min interval used to determine the PSD of the magnetic field fluctuations from FFT analysis is provided. Most intervals are confined within the BL, although some extended to the MSH or the MS, where more stable spectral peaks were observed. Observed fluctuation frequencies on both the dayside and nightside are not strong functions of either the upstream solar wind speed or LT, as shown in Figure 8. The dayside events have a nearly constant average frequency f~0.025 Hz under all conditions. The wave periods of nightside events, however, are well ordered by B_{MP}. As illustrated in Figure 8c, the observed frequency correlates with that of the Na^+ gyrofrequency, which varies from ~0.01 Hz to ~0.05 Hz in this region.

5. Discussion

The high content of planetary ions in the magnetotail at Mercury is analogous to the substantial amounts of keV O^+ ions sometimes present at Earth [*Lennartsson and Shelley*, 1986; *Kistler et al.*, 2006; *Liao et al.*, 2010]. The presence of oxygen ions in Earth's plasma sheet has been correlated with increased ionospheric

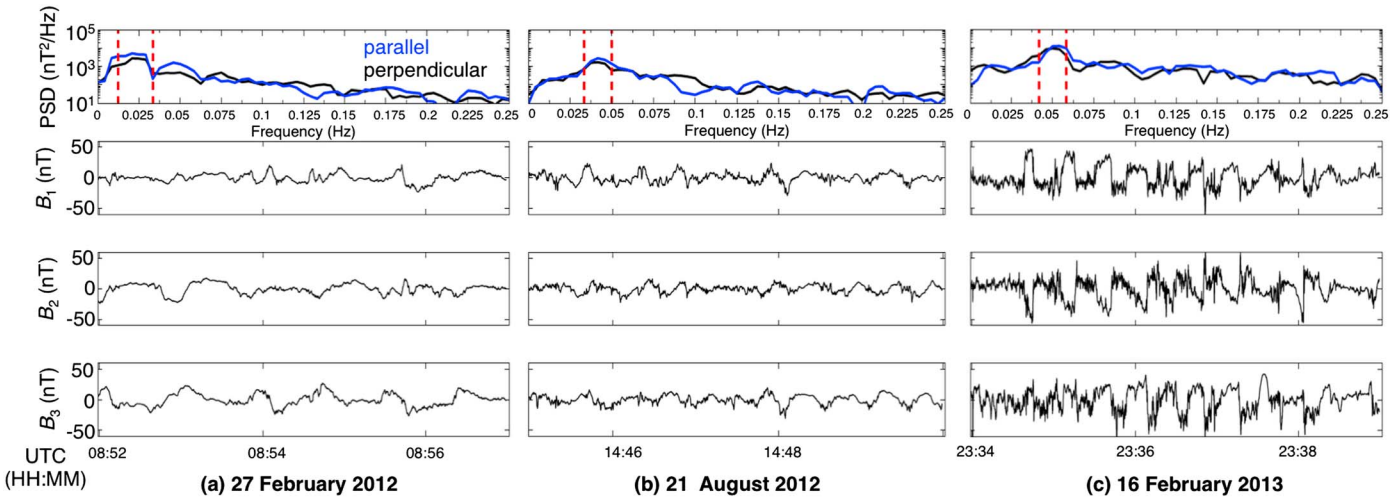

Figure 7. Same format as Figure 6 but for the nightside K-H events in Figure 5.

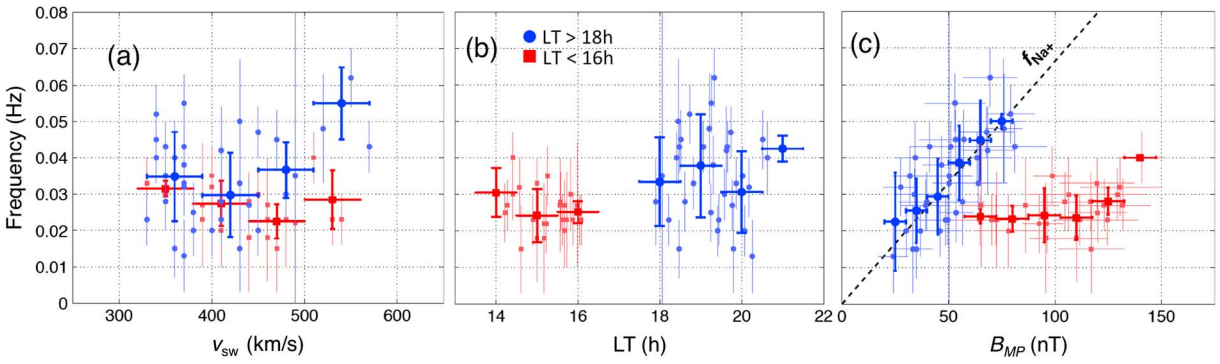

Figure 8. Observed frequency of peak magnetic field fluctuations as a function of (a) orbit-averaged upstream solar wind speed, (b) LT, and (c) B_{MP} for both dayside (red) and nightside (blue) events. For Figures 8a and 8b, the lighter-colored markers correspond to individual orbits, and the vertical error bars correspond to the FWHM of the observed spectral peak. Darker-colored markers indicate bin averages, and vertical and horizontal error bars correspond to the standard deviation of observed frequencies in each bin and bin width, respectively. For Figure 8c, lighter-colored markers correspond to individual orbits, and vertical and horizontal error bars correspond to the FWHM of the observed spectral peak and standard deviation of B_{MP} in the boundary layer, respectively. The Na^+ gyrofrequency is indicated by the black dashed line. The dayside events maintain a constant magnetic fluctuation frequency of ~0.025 Hz, whereas for the nightside events the frequency of magnetic fluctuations correlates with the Na^+ gyrofrequency, which varies from ~0.01 Hz to ~0.05 Hz.

outflow [*Nosé et al.*, 2009; *Winglee and Harnett* 2011; *Liu et al.*, 2013]. At Mercury, however, there is a strong asymmetry in the Na^+ content in the tail with respect to local midnight, and Na^+ fluxes nearly monotonically increase from dawn to dusk [*Raines et al.*, 2013]. If contributing to the local plasma mass density, Na^+ may influence the global configuration of the neutral *X* line, as well as the onset location of magnetotail reconnection. In a recent study of reconnection in Mercury's magnetotail, *DiBraccio et al.* [2015] found frequent formation of flux ropes having core fields that are highly skewed with respect to the Y_{MSM} direction but with no systematic pattern indicative of a global tilt. The size of these flux ropes was estimated to be a few H^+ gyroradii, much smaller than those of Na^+ ions near the duskside MP, suggesting that whereas gyrating Na^+ ions may scatter through interaction with these perturbations, it is unlikely that they influence flux rope formation. However, *DiBraccio et al.*'s [2015] study focused on events measured within only ~1 h of local midnight, where the overall variation in Na^+ content is not high and the number density of Na^+ in this region is on the order of ~1%.

The contribution of Na^+ ions to the plasma thermal pressure does not necessarily imply or require that these ions follow well-defined, closed drift paths. From models of Mercury's magnetic field and estimates of particle energies, the change in the magnetic moment associated with a transit of the cross-tail current sheet have been calculated for both H^+ and Na^+ [*Delcourt et al.*, 2003, 2007; *Korth et al.*, 2012]. These calculations predict chaotic scattering and meandering particle motion, i.e., Speiser-type orbits [*Speiser*, 1965; *Büchner and Zelenyi*, 1989], throughout nearly the entire magnetotail for both species. Such motion may result in precipitation of keV ions onto a large fraction of Mercury's nightside surface [*Seki et al.*, 2013]. Regardless of the presence of true "guiding center" drift motion in the tail even for H^+, ion gyration in these regions generates an opposing field that results in substantial diamagnetic depressions in *B*.

In a moderate β_i plasma, where β_i is the ratio of ion thermal pressure to magnetic pressure, even small ($T_\perp/T_\parallel < 2$) temperature anisotropies can drive ion cyclotron wave modes [*Gary et al.*, 1993]. From the limited Na^+ velocity distribution data alone, we cannot exclude the possibility that the observed fluctuations are the ion cyclotron wave mode. However, high fluxes of Na^+ ions have been measured in Mercury's magnetosphere without the presence of any fluctuations near the Na^+ gyrofrequency [*Raines et al.*, 2013, 2014; *Gershman et al.*, 2014]. Furthermore, the observed wave right-hand polarization, preference for northward IMF conditions, proximity to the MP, and nonsinusoidal sawtooth-like appearance of these events are highly suggestive that these events are associated with the K-H instability at Mercury.

In principle, K-H wave growth should be possible for both northward and southward IMF. However, we find that K-H vortex formation is much more likely under northward IMF conditions, i.e., $B_Z > 0$, consistent with previous studies at Mercury [*Sundberg et al.*, 2012; *Liljeblad et al.*, 2014]. Such an association with northward

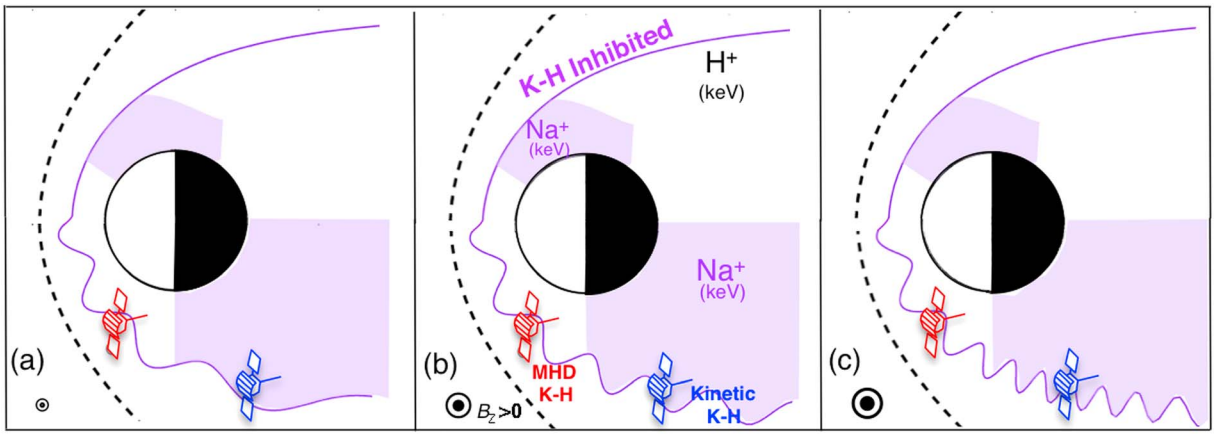

Figure 9. (left to right) Illustration of K-H wave growth along Mercury's MP boundary for increasing B_{MP} given a constant vortex speed. Toward the tail, where the Na^+ is expected to dominate the plasma mass density, the observed frequency of K-H waves (blue spacecraft) matches that of the Na^+ gyrofrequency, which can be (a) less than, (b) equal to, or (c) greater than that observed on the dayside (red spacecraft). Near the dusk terminator, vortices formed on the dayside and nightside should interact through merging, breaking, or secondary generation processes (not shown). Few comparable K-H events have been observed on Mercury's dawnside, a possible consequence of large gyroradius effects from keV Na^+ and H^+.

IMF is consistent with observations of K-H waves at Earth [*Hasegawa et al.*, 2004], although events during southward IMF conditions have been identified [*Hwang et al.*, 2011]. *Sundberg et al.* [2012] suggested that K-H formation under southward IMF may be suppressed by the propagation of FTEs formed on the dayside [*Hwang et al.*, 2011] or from substantial dayside reconnection. However, purely reconnection-associated disruption of K-H waves on the duskside of Mercury is difficult to demonstrate given the ubiquitous presence of FTEs [*Slavin et al.*, 2010b, 2012; *Imber et al.*, 2014] and near lack of dependence of dayside reconnection rate on magnetic shear angle [*DiBraccio et al.*, 2013].

On the dayside, the absence of a strong dependence of f_{KH} on solar wind speed may indicate that low-energy Na^+ ions that are below the FIPS energy range contribute to the mass density. The presence of ~100 eV Na^+ ions inside the BL but not in the MS proper in Figure 4c demonstrates that this population is probably present and likely energized through interaction with the K-H vortices. The density of these planetary ions, unlike plasma sheet H^+, should not scale with the solar wind density and consequently should have the strongest influence on v_o for higher solar wind speeds that are typically associated with lower plasma density. In addition, the dayside vortex wavelength could be a function of the upstream solar wind speed, but in the absence of reliable measurements of L, this relationship is difficult to examine.

Despite different apparent unstable wavelengths on either side of the dusk terminator (Figure 9), dayside K-H vortices should convect tailward and interact with those on the nightside through merging, breaking, and secondary generation processes. Such interactions may explain why "pristine" K-H events (e.g., Figure 4c) are confined to Mercury's dayside and why nightside events exhibit additional frequency structure in magnetic spectrograms (Figure 5). We cannot definitively exclude the possibility of a different Na^+ wave mode generated from propagation of dayside K-H vortices along the flank magnetopause. Furthermore, because we are limited to observations from only a single spacecraft, the dayside and nightside K-H vortices have never been measured simultaneously, and we thus cannot distinguish between scenarios in which they coexist or one forms at the expense of the other. Nevertheless, the observed MSH-MS mixing in these nightside events exhibits a scaling with B_{MP} not present in their dayside counterparts.

Numerical simulations predict large differences in the structure and growth of K-H vortices at the kinetic scale between positive (dusk) and negative (dawn) field-aligned vorticity cases [*Nakamura et al.*, 2010; *Paral and Rankin*, 2013]. The simulations of *Paral and Rankin* [2013], for example, show a dawn-dusk asymmetry in the formation of K-H waves in a system with Mercury-like geometry. However, they did not include the presence of planetary ions, and their simulations have K-H wave periods of ~10 s, a factor of ~2 smaller than most of those observed in Mercury's magnetosphere. The simulations of *Nakamura et al.*

[2010] showed that the gyromotion of ions on the dawnside may serve to broaden the BL, lower the K-H growth rate, and increase the wavelength of the fastest-growing wave mode. From 06:00 to 12:00 LT, the presence of large-gyroradii keV Na^+ ions [*Raines et al.*, 2013, 2014] may serve this purpose. The gyromotion of keV H^+ may have a similar effect along the dawn flanks. Therefore, kinetic scale effects may influence K-H vortex formation and evolution along the dawnside MP and the dusk flank (Figure 9). An MHD-scale description of the K-H instability may be appropriate only along the MP in the 12:00–18:00 LT quadrant.

6. Concluding Remarks

Although contributing only modestly (~10–30%) to the total plasma thermal pressure in Mercury's premidnight plasma sheet, the large m/q of Na^+ compared with that of H^+ results in an increase in the dominance of the local plasma mass density toward the duskside magnetotail. This transition is accompanied by an observed fundamental shift in the behavior of the K-H instability at Mercury. In the 18:00–24:00 LT quadrant, the K-H frequency and the Na^+ gyrofrequency are highly correlated. This correlation suggests a transition from the simpler, fluid-level (i.e., MHD) K-H waves on the dayside to kinetic scale on the nightside. Mercury's duskside MP therefore provides a multiscale laboratory for the study of the Kelvin-Helmholtz instability, producing vital data that contribute to our understanding of the interaction between the solar wind and the rich and diverse set of magnetospheric environments found in the solar system.

Appendix A: Wave Events Observed at Mercury With MESSENGER

The start time (UTC), location, local plasma properties, and magnetic field spectral properties of all identified K-H-like wave events are included here for MESSENGER transits through the dayside and nightside magnetopause boundary layer in Tables A1 and A2, respectively, as described in section 4. The dashes indicate that the relevant plasma parameters were not available for that particular event.

Table A1. List of Wave Events Observed Between 14:00 and 16:00 LT

	Near-MP Boundary Layer			Solar Wind/MSH		FFT Interval	
Date	Time (HH:MM)	LT (h)	B_{MP} (nT)	θ_Z (deg)	v_{sw} (km/s)	Time (HH:MM)	Peak (Hz)
15 May 2011	09:26–09:31	15.7	123.0 ± 13.3	12 ± 8	–	09:26	0.027 ± 0.007
10 Aug 2011	09:23–09:28	15.8	106.5 ± 19.0	9 ± 6	350	09:23	0.030 ± 0.010
16 Aug 2011	09:22–09:25	14.4	140.7 ± 11.5	16 ± 9	510	09:21	0.040 ± 0.007
7 Nov 2011	10:33–10:40	15.6	64.8 ± 11.9	13 ± 6	540	10:33	0.023 ± 0.007
8 Nov 2011	22:31–22:35	15.2	92.6 ± 7.7	7 ± 4	490	22:30	0.022 ± 0.008
11 Nov 2011	10:26–10:31	14.6	130.5 ± 18.5	23 ± 11	400	10:26	0.032 ± 0.008
1 Feb 2012	09:23–09:29	15.9	111.7 ± 12.8	15 ± 9	–	09:23	0.023 ± 0.007
2 Feb 2012	20:46–20:50	15.6	104.7 ± 11.3	9 ± 5	440	20:43	0.028 ± 0.008
4 Feb 2012	08:09–08:12	15.3	98.8 ± 8.8	6 ± 3	400	08:08	0.035 ± 0.008
5 Feb 2012	07:41–07:44	15.0	119.7 ± 17.4	11 ± 7	330	07:42	0.033 ± 0.007
28 Apr 2012	07:31–07:37	16.1	70.6 ± 9.6	8 ± 5	530	07:30	0.023 ± 0.007
29 Apr 2012	23:32–23:36	15.7	70.3 ± 8.2	11 ± 6	480	23:30	0.023 ± 0.013
30 Apr 2012	15:27–15:36	15.6	86.2 ± 15.9	16 ± 8	460	15:29	0.027 ± 0.013
26 Jul 2012	23:43–23:50	15.6	116.7 ± 12.2	26 ± 10	530	23:42	0.028 ± 0.008
28 Jul 2012	23:47–23:50	15.2	96.1 ± 7.7	8 ± 5	490	23:50	0.022 ± 0.008
29 Jul 2012	15:45–15:49	15.0	110.2 ± 15.0	16 ± 8	460	15:44	0.018 ± 0.012
29 Jul 2012	23:44–23:48	14.9	124.6 ± 14.4	20 ± 9	460	23:44	0.023 ± 0.007
31 Jul 2012	07:44–07:49	14.6	117.0 ± 15.5	24 ± 9	470	07:45	0.015 ± 0.012
1 Aug 2012	15:43–15:48	14.3	131.9 ± 12.9	30 ± 10	–	15:43	0.027 ± 0.007
1 Aug 2012	23:44–23:50	14.2	113.3 ± 20.7	25 ± 9	–	23:43	0.025 ± 0.008
20 Oct 2012	16:03–16:12	16.0	71.7 ± 14.1	23 ± 8	390	16:00	0.023 ± 0.007
21 Oct 2012	00:05–00:15	16.0	65.3 ± 10.2	15 ± 6	390	00:05	0.027 ± 0.017
22 Oct 2012	08:08–08:15	15.7	64.7 ± 13.2	6 ± 3	410	08:07	0.020 ± 0.010
24 Oct 2012	16:06–16:10	15.2	93.8 ± 7.6	11 ± 6	440	16:02	0.018 ± 0.015
27 Oct 2012	16:00–16:06	14.4	123.3 ± 19.5	41 ± 11	450	16:01	0.030 ± 0.007

Table A2. List of Wave Events Observed Between 18:00 and 21:00 LT[a]

	Near-MP Boundary Layer			Solar Wind/MSH		Plasma Sheet				FFT Interval	
Date	Time (HH:MM)	LT (h)	B_{MP} (nT)	θ_Z (deg)	v_{sw} (km/s)	n_{H+} (cm^{-3})	T_{H+} (MK)	n_{Na+} (cm^{-3})	T_{Na+} (MK)	Time (HH:MM)	Peak (Hz)
11 Jun 2011	12:26–12:37	19.3	69.2 ± 12.9	36 ± 9	550	2.4	11.0 ± 0.1	0.4 ± 0.1	23.6 ± 2.7	12:31	0.062 ± 0.008
12 Jun 2011	00:21–00:38	19.1	48.2 ± 13.6	34 ± 12	570	6.5	12.6 ± 0.1	1.1 ± 0.1	26.2 ± 1.6	00:30	0.043 ± 0.007
4 Sep 2011	07:48–08:01	20.3	23.6 ± 6.9	59 ± 14	370	4.3	4.8 ± 0.1	1.9 ± 0.3	4.7 ± 0.4	07:52	0.013 ± 0.010
4 Sep 2011	20:15–20:25	20.2	30.2 ± 8.5	45 ± 7	370	4.2	10.4 ± 0.1	0.2 ± 0.2	17.8 ± 5.6	20:19	0.032 ± 0.008
5 Sep 2011	20:21–20:31	19.8	34.2 ± 8.5	52 ± 9	–	5.1	10.7 ± 0.1	0.7 ± 0.2	8.4 ± 1.1	20:23	0.015 ± 0.012
6 Sep 2011	08:20–08:42	19.6	68.4 ± 12.3	17 ± 10	410	2.6	7.9 ± 0.1	0.8 ± 0.1	16.5 ± 1.6	08:16	0.042 ± 0.012
30 Nov 2011	09:07–09:21	20.6	35.1 ± 9.4	33 ± 24	360	4.7	7.1 ± 0.1	1.6 ± 0.2	12.9 ± 0.8	09:12	0.040 ± 0.010
1 Dec 2011	21:09–21:23	20.0	31.9 ± 8.1	47 ± 7	350	10.9	6.0	1.5 ± 0.2	9.0 ± 0.7	21:10	0.035 ± 0.008
2 Dec 2011	21:13–21:32	19.6	41.2 ± 9.4	15 ± 7	370	8.4	5.3	2.2 ± 0.2	10.7 ± 0.6	21:24	0.043 ± 0.007
3 Dec 2011	09:11–09:24	19.4	35.4 ± 8.3	31 ± 15	380	7.5	4.5	2.6 ± 0.3	6.7 ± 0.4	09:18	0.020 ± 0.007
3 Dec 2011	21:14–21:38	19.2	53.6 ± 7.9	20 ± 8	380	6.0	5.5 ± 0.1	2.6 ± 0.2	12.9 ± 0.6	21:16	0.025 ± 0.008
6 Dec 2011	09:08–09:22	18.2	48.6 ± 12.6	19 ± 3	330	8.5	9.8 ± 0.1	1.2 ± 0.2	10.4 ± 0.9	09:22	0.023 ± 0.007
27 Feb 2012	08:35–08:45	20.1	30.1 ± 5.0	65 ± 5	400	5.0	6.0 ± 0.1	1.4 ± 0.3	6.7 ± 0.7	08:51	0.020 ± 0.007
1 Mar 2012	19:39–19:49	18.8	65.6 ± 14.0	41 ± 17	370	6.8	8.4 ± 0.1	2.1 ± 0.2	11.8 ± 0.7	19:39	0.033 ± 0.007
2 Mar 2012	07:26–07:35	18.6	39.9 ± 13.3	53 ± 25	350	14.7	7.8	4.0 ± 0.2	9.0 ± 0.4	07:30	0.028 ± 0.008
2 Mar 2012	19:19–19:29	18.5	81.2 ± 15.1	22 ± 9	350	9.7	5.3	2.7 ± 0.2	13.3 ± 0.6	19:21	0.043 ± 0.007
26 May 2012	06:31–06:40	19.7	67.5 ± 14.5	28 ± 5	450	9.8	11.1 ± 0.1	2.0 ± 0.2	17.4 ± 1.1	06:32	0.047 ± 0.007
26 May 2012	22:15–22:45	19.4	46.1 ± 10.6	26 ± 5	450	6.2	10.9 ± 0.1	3.8 ± 0.3	11.8 ± 0.6	22:19	0.020 ± 0.007
27 May 2012	14:35–14:45	19.2	76.0 ± 8.7	54 ± 10	520	–	–	–	–	14:00	0.048 ± 0.015
21 Aug 2012	14:40–14:49	19.9	50.3 ± 7.8	41 ± 12	430	6.0	7.0 ± 0.1	1.1 ± 0.3	13.3 ± 1.5	14:46	0.033 ± 0.007
22 Aug 2012	14:40–14:51	19.4	44.7 ± 11.4	44 ± 8	410	2.0	10.4 ± 0.2	1.6 ± 0.4	7.8 ± 0.9	14:41	0.023 ± 0.007
25 Aug 2012	06:55–07:03	18.4	72.8 ± 9.6	33 ± 9	430	15.9	15.3 ± 0.1	1.2 ± 0.3	12.9 ± 1.4	06:55	0.050 ± 0.017
17 Nov 2012	22:58–23:12	19.8	39.3 ± 11.6	48 ± 14	440	4.1	16.6 ± 0.2	0.5 ± 0.2	18.7 ± 3.0	22:59	0.027 ± 0.007
18 Nov 2012	07:05–07:17	19.6	33.3 ± 9.1	99 ± 26	480	6.0	18.2 ± 0.2	0.4 ± 0.2	18.7 ± 3.2	07:14	0.030 ± 0.007
20 Nov 2012	23:10–23:18	18.5	35.5 ± 6.6	97 ± 17	360	9.1	8.7 ± 0.1	0.4 ± 0.3	8.4 ± 2.3	23:17	0.015 ± 0.008
21 Nov 2012	23:12–23:20	18.1	50.4 ± 10.9	50 ± 6	490	2.8	21.2 ± 0.3	2.7 ± 0.3	9.0 ± 0.7	23:21	0.035 ± 12.000
22 Nov 2012	7:10–7:20	17.9	56.6 ± 10.1	48 ± 9	410	9.5	11.6 ± 0.1	2.2 ± 0.6	3.8 ± 0.5	07:17	0.028 ± 0.012
11 Feb 2013	15:18–15:29	20.5	57.3 ± 5.9	82 ± 9	470	6.9 ± 0.1	15.2 ± 0.2	3.1 ± 0.3	19.6 ± 1.4	15:23	0.045 ± 0.008
14 Feb 2013	15:24–15:30	19.3	45.8 ± 9.0	65 ± 15	370	14.2 ± 0.1	8.4 ± 0.1	5.0 ± 0.6	8.7 ± 0.6	15:25	0.038 ± 0.008
14 Feb 2013	23:34–23:39	19.3	58.3 ± 15.2	45 ± 20	370	25.9 ± 0.1	15.3 ± 0.1	12.7 ± 0.5	9.7 ± 0.4	23:35	0.055 ± 0.008
16 Feb 2013	7:38–7:45	18.7	79.2 ± 11.2	38 ± 7	340	19.0 ± 0.1	10.8 ± 0.1	7.8 ± 0.5	12.1 ± 0.6	07:47	0.052 ± 0.008
16 Feb 2013	15:34–15:38	18.5	58.1 ± 18.2	29 ± 8	340	36.0 ± 0.1	9.0	3.1 ± 0.4	12.1 ± 1.0	15:37	0.045 ± 0.008
16 Feb 2013	23:35–23:43	18.4	63.8 ± 16.0	44 ± 13	340	38.1 ± 0.1	8.2	15.2 ± 0.4	13.3 ± 0.4	23:34	0.040 ± 0.007

[a]Plasma densities and temperatures have been included, when available, for H^+- and Na^+-group ions as (n_{H+},T_{H+}) and (n_{Na+},T_{Na+}), respectively.

Acknowledgments

We thank two anonymous reviewers for their thoughtful comments on an earlier draft. The data used in this work can be obtained from the Planetary Data System (http://pds.nasa.gov/). The MESSENGER project is supported by the NASA Discovery Program under contracts NAS5-97271 to The Johns Hopkins University Applied Physics Laboratory and NASW-00002 to the Carnegie Institution of Washington. D.J.G. is supported by an appointment to the NASA Postdoctoral Program at Goddard Space Flight Center, administered by Oak Ridge Associated Universities.

Yuming Wang thanks the reviewers for their assistance in evaluating this paper.

References

Anderson, B. J., M. H. Acuña, D. A. Lohr, J. Scheifele, A. Raval, H. Korth, and J. A. Slavin (2007), The Magnetometer instrument on MESSENGER, *Space Sci. Rev.*, *131*, 417–450.

Anderson, B. J., C. L. Johnson, H. Korth, M. E. Purucker, R. M. Winslow, J. A. Slavin, S. C. Solomon, R. L. McNutt Jr., J. M. Raines, and T. H. Zurbuchen (2011), The global magnetic field of Mercury from MESSENGER orbital observations, *Science*, *333*, 1859–1862, doi:10.1126/science.1211001.

Andrews, G. B., et al. (2007), The Energetic Particle and Plasma Spectrometer instrument on the MESSENGER spacecraft, *Space Sci. Rev.*, *131*, 523–556.

Benna, M., et al. (2010), Modeling of the magnetosphere of Mercury at the time of the first MESSENGER flyby, *Icarus*, *209*, 3–10, doi:10.1016/j.icarus.2009.11.036.

Boardsen, S. A., and J. A. Slavin (2007), Search for pick-up ion generated Na^+ cyclotron waves at Mercury, *Geophys. Res. Lett.*, *34*, L22106, doi:10.1029/2007GL031504.

Boardsen, S. A., T. Sundberg, J. A. Slavin, B. J. Anderson, H. Korth, S. C. Solomon, and L. G. Blomberg (2010), Observations of Kelvin-Helmholtz waves along the duskside boundary of Mercury's magnetosphere during MESSENGER's third flyby, *Geophys. Res. Lett.*, *37*, L12101, doi:10.1029/2010GL043606.

Boardsen, S. A., J. A. Slavin, B. J. Anderson, H. Korth, D. Schriver, and S. C. Solomon (2012), Survey of coherent 1 Hz waves in Mercury's inner magnetosphere from MESSENGER observations, *J. Geophys. Res.*, *117*, A00M05, doi:10.1029/2012JA017822.

Büchner, J., and L. M. Zelenyi (1989), Regular and chaotic charged-particle motion in magnetotail-like field reversals: 1. Basic theory of trapped motion, *J. Geophys. Res.*, *94*, 11,821–11,842, doi:10.1029/JA094iA09p11821.

Delamere, P. A., R. J. Wilson, S. Eriksson, and F. Bagenal (2013), Magnetic signatures of Kelvin-Helmholtz vortices on Saturn's magnetopause: Global survey, *J. Geophys. Res. Space Physics*, *118*, 393–404, doi:10.1029/2012JA018197.

Delcourt, D. C. (2013), On the supply of heavy planetary material to the magnetotail of Mercury, *Ann. Geophys.*, *31*, 1673–1679, doi:10.5194/angeo-31-1673-2013.

Delcourt, D. C., S. Grimald, F. Leblanc, J.-J. Berthelier, A. Millilo, A. Mura, S. Orsini, and T. E. Moore (2003), A quantitative model of the planetary Na^+ contribution to Mercury's magnetosphere, *Ann. Geophys.*, *21*, 1723–1736, doi:10.5194/angeo-21-1723-2003.

Delcourt, D. C., F. Leblanc, K. Seki, N. Terada, T. E. Moore, and M.-C. Fok (2007), Ion energization during substorms at Mercury, *Planet. Space Sci.*, *55*, 1502–1508, doi:10.1016/j.pss.2006.11.026.

DiBraccio, G. A., J. A. Slavin, S. A. Boardsen, B. J. Anderson, H. Korth, T. H. Zurbuchen, J. M. Raines, D. N. Baker, R. L. McNutt Jr., and S. C. Solomon (2013), MESSENGER observations of magnetopause structure and dynamics at Mercury, *J. Geophys. Res. Space Physics*, *118*, 997–1008, doi:10.1002/jgra.50123.

DiBraccio, G. A., et al. (2015), MESSENGER observations of flux ropes in Mercury's magnetotail, *Planet. Space Sci.*, doi:10.1016/j.pss.2014.12.016.

Faganello, M., F. Califano, F. Pegoraro, and T. Andreussi (2012), Double midlatitude dynamical reconnection at the magnetopause: An efficient mechanism allowing solar wind to enter the Earth's magnetosphere, *Europhys. Lett.*, *100*, 69001, doi:10.1209/0295-5075/100/69001.

Fairfield, D. H., and K. W. Behannon (1976), Bow shock and magnetosheath waves at Mercury, *J. Geophys. Res.*, *81*, 3897–3906, doi:10.1029/JA081i022p03897.

Gary, S. P. (1991), Electromagnetic ion/ion instabilities and their consequences in space plasmas: A review, *Space Sci. Rev.*, *56*, 373–415.

Gary, S. P., S. A. Fuselier, and B. J. Anderson (1993), Ion anisotropy instabilities in the magnetosheath, *J. Geophys. Res.*, *98*, 1481–1488, doi:10.1029/92JA01844.

Gershman, D. J., T. H. Zurbuchen, L. A. Fisk, J. A. Gilbert, J. M. Raines, B. J. Anderson, C. W. Smith, H. Korth, and S. C. Solomon (2012), Solar wind alpha particles and heavy ions in the inner heliosphere, *J. Geophys. Res.*, *117*, A00M02, doi:10.1029/2012JA017829.

Gershman, D. J., J. A. Slavin, J. M. Raines, T. H. Zurbuchen, B. J. Anderson, H. Korth, D. N. Baker, and S. C. Solomon (2013), Magnetic flux pileup and plasma depletion in Mercury's subsolar magnetosheath, *J. Geophys. Res. Space Physics*, *118*, 7181–7199, doi:10.1002/2013JA019244.

Gershman, D. J., J. A. Slavin, J. M. Raines, T. H. Zurbuchen, B. J. Anderson, H. Korth, D. N. Baker, and S. C. Solomon (2014), Ion kinetic properties in Mercury's premidnight plasma sheet, *Geophys. Res. Lett.*, *41*, 5740–5747, doi:10.1002/2014GL060468.

Glassmeier, K.-H., H.-U. Auster, and U. Motschmann (2007), A feedback dynamo generating Mercury's magnetic field, *Geophys. Res. Lett.*, *34*, L22201, doi:10.1029/2007GL031662.

Hasegawa, H., M. Fujimoto, T.-D. Phan, H. Rème, A. Balogh, M. W. Dunlop, C. Hashimoto, and R. TanDokoro (2004), Transport of solar wind into Earth's magnetosphere through rolled-up Kelvin-Helmholtz vortices, *Nature*, *430*, 755–758, doi:10.1038/nature02799.

Hwang, K.-J., M. M. Kuznetsova, F. Sahraoui, M. L. Goldstein, E. Lee, and G. K. Parks (2011), Kelvin-Helmholtz waves under southward interplanetary magnetic field, *J. Geophys. Res.*, *116*, A08210, doi:10.1029/2011JA016596.

Imber, S. M., J. A. Slavin, S. A. Boardsen, B. J. Anderson, H. Korth, R. L. McNutt Jr., and S. C. Solomon (2014), MESSENGER observations of large dayside flux transfer events: Do they drive Mercury's substorm cycle?, *J. Geophys. Res. Space Physics*, *119*, 5613–5623, doi:10.1002/2014JA019884.

Kabin, K., M. H. Heimpel, R. Rankin, J. M. Aurnou, N. Gómez-Pérez, J. Paral, T. I. Gombosi, T. H. Zurbuchen, P. L. Koehn, and D. L. DeZeeuw (2008), Global MHD modeling of Mercury's magnetosphere with applications to the MESSENGER mission and dynamo theory, *Icarus*, *195*, 1–15, doi:10.1016/j.icarus.2007.11.028.

Kistler, L. M., et al. (2006), Ion composition and pressure changes in storm time and nonstorm substorms in the vicinity of the near-Earth neutral line, *J. Geophys. Res.*, *111*, A11222, doi:10.1029/2006JA011939.

Korth, H., B. J. Anderson, J. M. Raines, J. A. Slavin, T. H. Zurbuchen, C. L. Johnson, M. E. Purucker, R. M. Winslow, S. C. Solomon, and R. L. McNutt Jr. (2011), Plasma pressure in Mercury's equatorial magnetosphere derived from MESSENGER Magnetometer observations, *Geophys. Res. Lett.*, *38*, L22201, doi:10.1029/2011GL049451.

Korth, H., B. J. Anderson, C. L. Johnson, R. M. Winslow, J. A. Slavin, M. E. Purucker, S. C. Solomon, and R. L. McNutt Jr. (2012), Characteristics of the plasma distribution in Mercury's equatorial magnetosphere derived from MESSENGER Magnetometer observations, *J. Geophys. Res.*, *117*, A00M07, doi:10.1029/2012JA018052.

Korth, H., B. J. Anderson, D. J. Gershman, J. M. Raines, J. A. Slavin, T. H. Zurbuchen, S. C. Solomon, and R. L. McNutt Jr. (2014), Plasma distribution in Mercury's magnetosphere derived from MESSENGER Magnetometer and Fast Imaging Plasma Spectrometer observations, *J. Geophys. Res. Space Physics*, *119*, 2917–2932, doi:10.1002/2013JA019567.

Lee, L. C., R. K. Albano, and J. R. Kan (1981), Kelvin-Helmholtz instability in the magnetopause-boundary layer region, *J. Geophys. Res.*, *86*, 54–58, doi:10.1029/JA086iA01p00054.

Lennartsson, W., and E. G. Shelley (1986), Survey of 0.1- to 16-keV/e plasma sheet ion composition, *J. Geophys. Res.*, *91*, 3061–3076, doi:10.1029/JA091iA03p03061.

Liao, J., L. M. Kistler, C. G. Mouikis, B. Klecker, I. Dandouras, and J.-C. Zhang (2010), Statistical study of O^+ transport from the cusp to the lobes with Cluster CODIF data, *J. Geophys. Res.*, *115*, A00J15, doi:10.1029/2010JA015613.

Liljeblad, E., T. Sundberg, T. Karlsson, and A. Kullen (2014), Statistical investigation of Kelvin-Helmholtz waves at the magnetopause of Mercury, *J. Geophys. Res. Space Physics*, *119*, 9670–9683, doi:10.1002/2014JA020614.

Liu, Y., L. M. Kistler, C. G. Mouikis, B. Klecker, and I. Dandouras (2013), Heavy ion effects on substorm loading and unloading in the Earth's magnetotail, *J. Geophys. Res. Space Physics*, *118*, 2101–2112, doi:10.1002/jgra.50240.

Masters, A., et al. (2010), Cassini observations of a Kelvin-Helmholtz vortex in Saturn's outer magnetosphere, *J. Geophys. Res.*, *115*, A07225, doi:10.1029/2010JA015351.

Nakamura, T. K. M., H. Hasegawa, and I. Shinohara (2010), Kinetic effects on the Kelvin-Helmholtz instability in ion-to-magnetohydrodynamic scale transverse velocity shear layers: Particle simulations, *Phys. Plasmas*, *17*, 042119, doi:10.1063/1.3385445.

Ness, N. F., K. W. Behannon, R. P. Lepping, Y. C. Whang, and K. H. Schatten (1974), Magnetic field observations near Mercury: Preliminary results, *Science*, *185*, 151–160.

Nosé, M., A. Ieda, and S. P. Christon (2009), Geotail observations of plasma sheet ion composition over 16 years: On variations of average plasma ion mass and O^+ triggering substorm model, *J. Geophys. Res.*, *114*, A07223, doi:10.1029/2009JA014203.

Ogilvie, K. W., J. D. Scudder, R. E. Hartle, G. L. Siscoe, H. S. Bridge, A. J. Lazarus, J. R. Asbridge, S. J. Bame, and C. M. Yeates (1974), Observations at Mercury encounter by the plasma science experiment on Mariner 10, *Science*, *185*, 145–151, doi:10.1126/science.185.4146.145.

Paral, J., and R. Rankin (2013), Dawn-dusk asymmetry in the Kelvin-Helmholtz instability at Mercury, *Nat. Commun.*, *4*, 1645, doi:10.1038/Ncomms2676.

Raines, J. M., J. A. Slavin, T. H. Zurbuchen, G. Gloeckler, B. J. Anderson, D. N. Baker, H. Korth, S. M. Krimigis, and R. L. McNutt Jr. (2011), MESSENGER observations of the plasma environment near Mercury, *Planet. Space Sci.*, *59*, 2004–2015, doi:10.1016/j.pss.2011.02.004.

Raines, J. M., et al. (2013), Distribution and compositional variations of plasma ions in Mercury's space environment: The first three Mercury years of MESSENGER observations, *J. Geophys. Res. Space Physics*, *118*, 1604–1619, doi:10.1029/2012JA018073.

Raines, J. M., D. J. Gershman, J. A. Slavin, T. H. Zurbuchen, H. Korth, B. J. Anderson, and S. C. Solomon (2014), Structure and dynamics of Mercury's magnetospheric cusp: MESSENGER measurements of protons and planetary ions, *J. Geophys. Res. Space Physics*, *119*, 6587–6602, doi:10.1002/2014JA020120.

Russell, C. H., D. N. Baker, and J. A. Slavin (1988), The magnetosphere of Mercury, in *Mercury*, edited by F. Vilas, C. R. Chapman, and M. S. Matthews, pp. 514–561, Univ. of Ariz. Press, Tucson, Ariz.

Schriver, D., et al. (2011), Quasi-trapped ion and electron populations at Mercury, *Geophys. Res. Lett.*, *38*, L23103, doi:10.1029/2011GL049629.
Seki, K., N. Terada, M. Yagi, D. C. Delcourt, F. Leblanc, and T. Ogino (2013), Effects of the surface conductivity and the IMF strength on the dynamics of planetary ions in Mercury's magnetosphere, *J. Geophys. Res. Space Physics*, *118*, 3233–3242, doi:10.1002/jgra.50181.
Slavin, J. A., et al. (2010a), MESSENGER observations of extreme loading and unloading of Mercury's magnetic tail, *Science*, *329*, 665–668, doi:10.1126/science.1188067.
Slavin, J. A., et al. (2010b), MESSENGER observations of large flux transfer events at Mercury, *Geophys. Res. Lett.*, *37*, L02105, doi:10.1029/2009GL041485.
Slavin, J. A., et al. (2012), MESSENGER observations of a flux-transfer-event shower at Mercury, *J. Geophys. Res.*, *117*, A00M06, doi:10.1029/2012JA017926.
Solomon, S. C., et al. (2001), The MESSENGER mission to Mercury: Scientific objectives and implementation, *Planet. Space Sci.*, *49*, 1445–1465, doi:10.1016/S0032-0633(01)00085-X.
Speiser, T. W. (1965), Particle trajectories in model current sheets: 1. Analytical solutions, *J. Geophys. Res.*, *70*, 4219–4226, doi:10.1029/JZ070i017p04219.
Spreiter, J. R., A. L. Summers, and A. Y. Alksne (1966), Hydromagnetic flow around the magnetosphere, *Planet. Space Sci.*, *14*, 223–253, doi:10.1016/0032-0633(66)90124-3.
Sundberg, T., S. A. Boardsen, J. A. Slavin, L. G. Blomberg, and H. Korth (2010), The Kelvin-Helmholtz instability at Mercury: An assessment, *Planet. Space Sci.*, *58*, 1434–1441, doi:10.1016/j.pss.2010.06.008.
Sundberg, T., S. A. Boardsen, J. A. Slavin, B. J. Anderson, H. Korth, T. H. Zurbuchen, J. M. Raines, and S. C. Solomon (2012), MESSENGER orbital observations of large-amplitude Kelvin-Helmholtz waves at Mercury's magnetopause, *J. Geophys. Res.*, *117*, A04216, doi:10.1029/2011JA017268.
Trávníček, P. M., D. Schriver, P. Hellinger, D. Herčík, B. J. Anderson, M. Sarantos, and J. A. Slavin (2010), Mercury's magnetosphere-solar wind interaction for northward and southward interplanetary magnetic field: Hybrid simulation results, *Icarus*, *209*, 11–22, doi:10.1016/j.icarus.2010.01.008.
Uritsky, V. M., J. A. Slavin, G. V. Khazanov, E. F. Donovan, S. A. Boardsen, B. J. Anderson, and H. Korth (2011), Kinetic-scale magnetic turbulence and finite Larmor radius effects at Mercury, *J. Geophys. Res.*, *116*, A09236, doi:10.1029/2011JA016744.
Wang, Y.-C., J. Mueller, U. Motschmann, and W.-H. Ip (2010), A hybrid simulation of Mercury's magnetosphere for the MESSENGER encounters in year 2008, *Icarus*, *209*, 46–52, doi:10.1016/j.icarus.2010.05.020.
Wilson, R. J., P. A. Delamere, F. Bagenal, and A. Masters (2012), Kelvin-Helmholtz instability at Saturn's magnetopause: Cassini ion data analysis, *J. Geophys. Res.*, *117*, A03212, doi:10.1029/2011JA016723.
Winglee, R. M., and E. Harnett (2011), Influence of heavy ionospheric ions on substorm onset, *J. Geophys. Res.*, *116*, A11212, doi:10.1029/2011JA016447.
Winslow, R. M., C. L. Johnson, B. J. Anderson, H. Korth, J. A. Slavin, M. E. Purucker, and S. C. Solomon (2012), Observations of Mercury's northern cusp region with MESSENGER's Magnetometer, *Geophys. Res. Lett.*, *39*, L08112, doi:10.1029/2012GL051472.
Winslow, R. M., et al. (2014), Mercury's surface magnetic field determined from proton-reflection magnetometry, *Geophys. Res. Lett.*, *41*, 4463–4470, doi:10.1002/2014GL060258.
Zurbuchen, T. H., J. M. Raines, G. Gloeckler, S. M. Krimigis, J. A. Slavin, P. L. Koehn, R. M. Killen, A. L. Sprague, R. L. McNutt Jr., and S. C. Solomon (2008), MESSENGER observations of the composition of Mercury's ionized exosphere and plasma environment, *Science*, *321*, 90–92, doi:10.1126/science.1159314.
Zurbuchen, T. H., et al. (2011), MESSENGER observations of the spatial distribution of planetary ions near Mercury, *Science*, *333*, 1862–1865, doi:10.1126/science.1211302.